RSC Advances

ROYAL SOCIETY OF CHEMISTRY

www.rsc.org/advances

Analysis of electron transfer dynamics in mixed community electroactive microbial biofilms

Bernardino Virdis,[1,2]* Diego Millo,[3] Bogdan C. Donose,[1,2] Yang Lu,[2] Damien J. Batstone,[2] Jens O. Krömer[1,2]

1 The University of Queensland, Centre for Microbial Electrochemical Systems (CEMES), Level 4, Gehrmann Building (60), Brisbane, QLD 4072, Australia.

2 The University of Queensland, Advanced Water Management Centre (AWMC), Level 4, Gehrmann Building (60), Brisbane, QLD 4072, Australia.

3 Biomolecular Spectroscopy/LaserLaB Amsterdam, Vrije Universiteit Amsterdam, De Boelelaan 1081, NL-1081 HV Amsterdam, The Netherlands

* E-mail: b.virdis@uq.edu.au

Keywords: bioelectrochemical systems, confocal resonance Raman microscopy, electron transfer, cytochromes, biofilms.

Abstract

Mixed community electroactive organisms form multi-layered biofilms that are able to produce current densities comparable to those of pure *Geobacter sulfurreducens*, an extensively studied metal-reducing organism. The long-range electron transfer (ET) inside the biofilms and at the biofilm/electrode interface was proven to be promoted by a network of outer membrane cytochromes (OMCs). In the present work, we investigate the electron transfer process in mixed community biofilms grown on Indium Tin Oxide (ITO) electrodes by combining electrochemical measurements with Confocal Resonance Raman Microscopy (CRRM) under potentiostatic control and during chronoamperometry (CA). This approach allowed direct comparison of the heterogeneous redox process at the biofilm/electrode interface with the long-range OMCs-mediated ET inside the bulk biofilm. Our work shows that: (i) during substrate oxidation, all OMCs are in the reduced state at any distance from the electrode, and no concentration gradient of oxidized OMCs is observed; (ii) the rate constant for the long-range, homogeneous ET (k^0_{hom}) is 0.028 s^{-1}, which is considerably lower than that predicted by others under the hypothesis that homogeneous ET is promoted by OMCs alone, and may thus indicate the contribution of alternative fast electron transfer processes; (iii) the metabolic respiration rate is much faster compared to both homogeneous and heterogeneous ET, which have similar rate constants. All in all, our results suggest that differences exist in electron transfer mechanisms between mixed community and *G. sulfurreducens* electroactive biofilms.

Introduction

Investigation of electron transfer (ET) mechanisms in electroactive microbial biofilms (that is, biofilm capable of extracellular electron communication with electrodes) has motivated substantial research efforts in recent years. Unraveling electron conduction in microbes is relevant not only to engineered devices such as biosensors and bioelectrochemical systems, but it can also

help explaining important microbial physiological processes governing natural geochemical cycles in sediments. Amongst the most studied microbial players in electroactive biofilms are bacteria belonging to the genus *Geobacter* and *Shewanella*, because of the high current densities achievable at electrodes, and their importance as model organisms of ET modes, respectively. *Geobacter sulfurreducens* can develop thick biofilms on electrode surfaces, spanning distances exceeding 100 μm. The mechanisms by means of which electrons are transported through such long distances is the subject of significant debate.[1-3] Proposed models include a) redox conduction, that is, electron transfer through incoherent multistep electron hopping between discrete redox cofactors bound to the biofilms,[4] b) metallic-like conductivity, according to which electron transfer occurs through intrinsic conducting properties of extracellular appendages (called nanowires) specific to *Geobacter sulfurreducens*.[5] Redox conduction is based on the relatively high abundance of multiheme *c*-type cytochromes located on the outer membrane and periplasmic space, as well as along extracellular filaments, and dispersed in the extracellular polymeric substance.[6] On the contrary, metallic-like conduction excludes hopping between cytochromes,[7,8] since the inter-heme spacing - measured by immune-gold labelling outside of the bioelectrochemical system - is too large for electron hopping to occur.[9] While sufficient structural information regarding the spatial organization of heme-proteins in biofilms under physiologically relevant conditions is still missing, independent electrochemical and spectroscopy measurements seems to agree on the important role played by *c*-type cytochromes in wiring the electroactive biofilms to electrodes and providing electric conductivity.[1,10-21]

Redox conduction is described by a detailed model consisting of a fast heterogeneous electron transfer at the biofilm/electrode interface governed by electron tunnelling, coupled with a slower long-range homogeneous electron transfer occurring via a hopping mechanism.[17,18] This model requires a redox gradient as driving force to allow ET to a given direction.[22] Recently, Bonanni *et al*.[23] proposed a model where the contribution of both OMCs and nanowires are considered. While this seems to explain electron conduction in *G. sulfurreducens* biofilms, electron transfer may be different in mixed culture

films, where the presence of multiple species may add complexity to the already complicated spectrum of synergies and competitions that are expected to arise for available substrates and the terminal electron acceptor (*i.e.*, the anode). While studying conduction in model organisms such as *G. sulfurreducens* is important from a physiological and mechanistic point of view, understanding ET in broader mixed culture microbial aggregates is essential also because of the role they play in existing and potential applications in environmental and industrial biotechnologies.[24-26]

Spectroelectrochemical methods that derive from the combination of electrochemical techniques with various spectroscopies provide great opportunities for the study of electron conduction in these systems. Compared to established electrochemical methods such as cyclic voltammetry (CV), techniques based on Raman scattering provide important structural information of the matrix based on spectral fingerprint of key molecules.[27] Resonance Raman (RR) spectroscopy is particularly suitable for the study of electron transfer involving cytochromes because of the signal enhancement achieved when the frequency of the excitation laser line is in proximity to an electronic transition of the heme group in a cytochrome. This selectivity towards heme-containing proteins together with the spatial resolution achievable by combining RR spectroscopy with microscopy (yielding confocal resonance Raman microscopy, CRRM), allows the use of CRRM to monitor surface-exposed cytochromes promoting the long-range ET at any distance from the electrode surface, as well as periplasmic cytochromes involved in cells metabolism and extracellular ET. However, due to their abundance and accessibility, surface-exposed proteins, hereby denoted as OMCs, dominate the spectrum.[13] Using this approach, we have previously resolved the spatial distribution[28] and redox state[20] of OMCs of biofilms *in vivo*, without impacting on the catalytic activity of mixed culture biofilms.

Herein, we improved our experimental set up and devised a miniature spectroelectrochemical cell (schematized in Figure S1) equipped with transparent Indium Tin Oxide (ITO) working electrodes specifically designed to allow simultaneous electrochemical and CRRM measurements on the biofilms directly (that is, *in situ*) without the need to transfer the biofilm/electrodes from the electrochemical cell to the microscope stage; a

procedure that inevitably exposes the biofilms to air, albeit briefly. This new set up allows to compare our results on mixed cultures to what others have done on *G. sulfurreducens* biofilms.[16] This approach excludes that differences observed for mixed cultures and *G. sulfurreducens* are due to the experimental configuration such as the focusing of the laser beam and the electrode material. Moreover, CRRM hereby applied in the time-resolved mode, was used to support the interpretation of simultaneous chronoamperometry (CA) and CRRM measurements. To our knowledge, this combined approach was never attempted before, and it turned out to provide much direct information about the rate limiting steps of electron transfer processes in electroactive microbial biofilms.

Material and Methods

Biofilms formation and growth medium

Primary biofilms were enriched using domestic wastewater from a local wet well as the inoculum and incubated in a sealed single-chambered bioelectrochemical system consisting of two carbon rods (Morgan AM&T, Australia) serving as working and counter electrodes, and a Ag/AgCl reference electrode in 3 M KCl (MF-2052, Basi, USA). All potentials herein are reported with respect to this reference electrode (+0.210 V *vs* the standard hydrogen electrode, SHE). The electrodes were immersed into 400 mL sterile anaerobic media (composition below) purged with pure nitrogen for at least 30 minutes to ensure anoxic conditions. The working electrode was poised at 0 V using a potentiostat (Potentiostat/Galvanostat VMP3, BioLogic Science Instruments, France). Biofilm growth was monitored by measurement of bioelectrocatalytic current production and by regular cyclic voltammetry analysis. The media was regularly exchanged (usually once per week). Primary biofilms were scraped off the rods using a sterile blade and used as inoculum for the formation of secondary biofilms that were used in this study. Both primary and secondary biofilms were grown at room temperature (22±1)°C. The growth medium consisted of autoclaved deionized water containing: Na_2HPO_4 (6.0 g L^{-1}), KH_2PO_4 (3.0 g L^{-1}), NH_4Cl (0.1 g L^{-1}), NaCl (0.5 g L^{-1}), $MgSO_4 \cdot 7H_2O$ (0.1 g L^{-1}), $CaCl_2 \cdot 2H_2O$ (0.015 g L^{-1}), trace

elements solution (1 mL L^{-1}, composition in Lu *et al.*[29]). Sodium acetate (CH_3COONa) was used as metabolic substrate at concentrations that ranged between 1 and 20 mM as indicated in the text.

Spectroelectrochemical cells

The spectroelectrochemical cells used for CRRM measurements were designed to allow for observations of electroactive biofilms *in vivo* and *in situ*. A schematic cell is provided in Figure S1 in the Supplementary Information (SI). It consists of single chambered miniature BESs obtained by etching a 10 x 10 mm well into a 10 mm thick polycarbonate frame. Small channels were drilled on the sides of the frame to accommodate the reference electrode and the counter electrode (consisting of a platinum wire). The working electrode consisted of 20 x 20 mm sodalime glass cover slip (thickness 0.5 mm) coated with 100 nm of Indium Tin Oxide (ITO 90/10 wt%, 99.99%, Testbourne Ltd., UK) deposited using an electron beam evaporator (BJD2000, Temescal, USA). The use of ITO permitted to perform confocal analysis directly from the outside of the electrochemical cells, without the need to remove the biofilm from the medium and expose it to air, albeit for a brief period of time. The glass/ITO sandwich was plasma-treated to render the surface highly hydrophilic and favour bacterial attachment,[30] and it was then glued onto one side of the well using silicone glue, resulting in an effective (exposed) area of the electrode of 1 cm^2. Finally, a glass cover slip was glued to the opposite side of the well to close the electrochemical chamber, resulting in an internal volume of 1 mL. The electrochemical cells were fed using a multichannel syringe pump (NE-1600, New Era Pump Systems, USA) at the flow rate ranging from 0.1 to of 1 mL h^{-1}. External connection of the ITO was obtained by gluing titanium wires on the portion of the ITO layer outside of the chamber using conductive epoxy glue (MG chemicals, USA). Working, counter, and reference electrodes were typically connected to a multichannel potentiostat (CHI1000B, CH Instruments, USA). For electrochemical measurements during Raman spectra acquisition, a VMP3 Potentiostat/Galvanostat (BioLogic Science Instruments, France) was used. Biofilms were grown at a potential of 0 V. Measurements of catalytic current production over time and of cyclic

voltammograms were used to monitor the electrochemical activity of the biofilms.

Confocal Resonance Raman Microscopy measurements

All CRRM measurements were performed at room temperature (22±1°C) using an Alpha 300 Raman/AFM (WITec GmbH, Ulm, Germany) equipped with a frequency-doubled continuous-wave Nd:YAG laser to obtain a 532 nm excitation line. The laser beam was focused by an objective lens (Nikon 40X, N.A. 0.6, CFI S Plan Fluor ELWD objective). The back-scattered Raman light from the sample was collected with a 100 μm optical fibre employing a Raman spectrometer (1800 grooves per mm grating) with a charge-coupled device (EMCCD) spectroscopic detector. Biofilm stability upon exposure to the 532 nm laser was tested by measuring changes of the signal intensity of the vibrational mode ν_{15} (sensitive to *c*-type heme groups, *vide infra*) at 750 cm^{-1} during a 300 s continuous exposure test (Figure S2). Measurements confirmed that changes of signal intensity for the mode ν_{15} were negligible (<2.4 CCD counts s^{-1}) for laser powers less than 430 μW (measured at the sample using a power meter (Thor Labs, USA)). Project FOUR software (WITec GmbH, Ulm, Germany) was used for spectra processing and image reconstruction. OriginPro 9.1 software (OriginLab, Northampton, USA) was used for data fitting. Depth measurements on biofilm sections were done by collecting individual spectra over a total of 12 points spaced 5 μm from each other each (covering 60 μm-thick sections), and using an integration time of 20 s per point (refer to the SI for additional information regarding this measurement).

Time-resolved simultaneous CRRM and CA measurements were conducted by continuously collecting RR spectra from a single biofilm location 5 μm in depth from the electrode surface. During the tests, the potential of the working electrode was stepped from an initial value (E_i) to a final value (E_f) to perturb the original redox equilibrium E_i. While E_i was set at -0.5 V, *Ef* of -0.2 V, 0 V, and +0.2 V where used. The E_i was kept for a total of 300 s, after which the potential was instantaneously shifted to the E_f and kept for additional 240 s. The subsequent relaxation profiles of current and intensity of the Raman vibrational mode ν_{15} at about 750 cm^{-1} (used as marker for the redox state of

OMCs[20]) was used to monitor the redox processes occurring during the potential step experiment. To avoid over exposure of the biofilm to the laser beam, the collection of the RR spectra started at t = 240 s, that is, 60 s before the transition, and continued for the remaining of the test. Spectral acquisition was done at integration time of 0.2 s. To further confirm the redox state of the probed OMCs, additional experiments were carried out where single spectra were collected during 60 s prior to the transition, and then again 180 s after the transition. The integration time for these tests was 60 s.

Results and Discussion

Analysis of the voltammetric response of electroactive biofilms

Biofilms were incubated at a potential of 0 V until stable catalytic substrate oxidation was achieved as indicated by current profiles (data not shown). Confocal laser scanning microscopy (CLSM) micrographs using Fluorescent *in situ* Hybridization (FISH) labeling showed the electroactive organisms forming a homogeneous coverage of the electrode surface with an average thickness of (17±4) μm (Figure S5). Analysis of the individual cell clusters scraped off the electrode confirmed the presence of *Geobacter spp*. (Text S2). The voltammetric response of the biofilms was monitored under both turnover and non-turnover conditions, that is, in the presence and in the absence of the metabolic substrate acetate, respectively. Typical voltammograms are reported in Figure 1. Measurements in turnover conditions revealed the presence of one catalytic redox-active site E^f centered at -0.350 V. This value is very close to the arithmetic average ($E_{1/2}$ at -0.346 V) of the two redox couples $E^{f,1}$ and $E^{f,2}$ obtained under non-turnover conditions and centered at formal potentials of -0.389 V and -0.303 V, respectively, thus suggesting the involvement of both redox couples in the catalytic current. This voltammetric response has been typically observed in *Geobacter* enriched electroactive biofilms on graphite, roughened silver and glassy carbon,[14,20,31] demonstrating that ITO represents a suitable electrode material for electroactive biofilms, as previously shown by others.[12,13,16,32,33]

Analysis of the RR spectra of biofilms in completely reduced or oxidized electrochemical conditions in the absence of metabolic substrate

The spectroelectrochemical cells used in this study allowed for CRRM measurements to be performed directly on the biofilms in their culturing media without the need to expose them to air while transferring onto the microscope stage. This represented a major advancement from our previous set ups.[20,28] The use of transparent ITO electrodes deposited on a glass substrate (0.5 mm thick cover slip), allowed for the Raman observations to be performed non-invasively from the outside of the spectroelectrochemical cell, providing minimal disturbance to the biofilms.

RR spectra of biofilms collected under potentiostatic conditions in the absence of acetate are reported in Figure 2. Bands assignment is depicted in Table 1. Consistently to what we reported previously, the vibrational bands ascribed to *c*-type heme groups of the cytochromes embedded in the biofilms dominate the RR spectra.[20] The mode ν_{15}, observed at around 750 cm^{-1} is ascribed to the pyrrole breathing. The intensity of this band is proportional not only to the presence of *c*-type hemes,[34] but also to the amount of cytochromes in the reduced state.[20,35-37] Modes in the mid-frequency region (1100-1700 cm^{-1}), ascribed primarily to stretching vibrations of the porphyrin ring, are indicative of oxidation-, spin-, and coordination-state of the Fe atom.[38] With the anode poised at 0 V – hence more positive than the average of the macroscopic redox potentials $E_{1/2}$ as determined by non-turnover voltammetry discussed above - the modes ν_{21}, ν_4, ν_{20}, ν_2, and ν_{10} were centered respectively at 1316, 1369, 1400, 1583, and 1635 cm^{-1} and a shoulder appeared in correspondence of the mode ν_{11} at 1563 cm^{-1}, consistently with an oxidized heme group. Conversely, the application the negative potential of -0.6 V (*i.e.*, more negative than the $E_{1/2}$) caused the modes ν_{21}, ν_4, and ν_{20}, to downshift to 1310, 1360, 1391, respectively, while the ν_3 (not resolvable at 0 V) appeared at 1496 cm^{-1}. The mode ν_{10} did not shift although it reduced considerably its intensity, and the mode ν_{11} was no longer resolvable. The band ν_{15} also did not shift in position, but its intensity was considerably enhanced by the application of the negative potential. These changes are consistent with an oxidized (at 0 V) and reduced (at -0.6 V) heme group

having a six-coordinated iron atom in low-spin state. Even if mixed culture biofilms on graphite, glassy carbon and silver display the typical His-Fe-His axial ligation in both oxidation states,[14,20,28] our data on ITO show a different axial ligation at different oxidation states. In fact, while the ν_3 of the reduced state is consistent with the His-Fe-His axial ligation, the ν_4 and the ν_{10} of the oxidized heme at 1369 and 1635 cm^{-1} indicate the His-Fe-Met axial ligation.[39] This is the first time such a ligation is observed for mixed culture biofilms. However, since CRRM spectra ascribable to the His-Fe-Met ligation were reported by others for oxidized *G. sulfurreducens* biofilms on ITO,[16] we argue that the electrode material we used contributed to select those bacterial species displaying the same axial ligation as *G. sulfurreducens* on the same electrode material. This observation reinforces the conclusions of a recent report on the impact of surface composition on the redox properties of microbial biofilms.[40]

Measurements of the redox state of cytochromes across biofilm sections in the presence of metabolic substrate

The RR spectra recorded under non-turnover condition at the extreme potentials of -0.6 V and 0 V will serve as reference spectra for the reduced and the oxidized OMCs, respectively. In fact, the spectra discussed in this study do not deviate from those shown in Figure 2 significantly. For this reason, a qualitative assignment of the dominant redox state is possible by tracking the spectral position of redox-sensitive vibrational modes ν_{15}, ν_{21}, ν_4, ν_{20}, ν_3, and ν_{10}, without the need to adopt laborious fitting procedures. The knowledge of the redox state of OMCs in actively respiring biofilms have been subject of intense research in recent years, since it provides important information on the rate-limiting steps controlling the catalytic current generation in electroactive biofilms. According to the redox conduction model developed by Strycharz and coworkers for a system not limited by ET at the biofilm/electrode interface (that is, a system where the ET rate constant for heterogeneous electron transfer, k_{het}, is very large), in the presence of oxidizing electrode potential, the RR spectra of a metabolizing biofilm is expected to include the contribution of oxidized cytochromes, and the

establishment of a measurable redox gradient.[18] This was recently reported for *G. sulfurreducens* biofilms studied with confocal Raman spectroscopy.[11,16]

To study possible local changes of redox state for OMCs in our mixed community biofilms, we used the confocal capabilities of our system to collect RR spectra from different focal planes within the biofilms. We performed measurements with the anode poised at the potentials of 0 V and 0.2 V, and in the presence of different levels of acetate (*i.e.*, 1 mM, 5 mM, and 20 mM). Each spectrum was acquired sequentially every 5 μm across a 60 μm long line extending in the Z-direction (starting from the electrode surface), using an integration time of 20 seconds. An example of a redox profiling measurements in the presence of 20 mM acetate and with the anode poised at 0.2 V is included in the SI, together with additional details on the measurement (Text S1). Each spectrum was evaluated individually to assess the position of the redox marker bands ν_{21}, ν_4, and ν_{20}, which are ascribed to the largest spectral shifts upon changes in redox state (*vide supra*). Per each set of experiments, the respective spectral positions were grouped and averaged per discrete depth step (5 μm). Actual values are summarized in Table S1 and S2 in the SI, while Figure 3 shows a visual representation of the results. In fact, the figure depicts the average positions of the modes ν_{21}, ν_4, and ν_{20} at increasing distances from the electrode surface. In order to assist the assessment of the redox state, the figure also reports the average position of the bands ν_{21}, ν_4, and ν_{20} recorded in non-turnover conditions with the anode poised at 0 V or -0.6 V (attributed to OMCs in completely oxidized or reduced state, respectively), thus depicting the full range of variations for these redox markers upon shifts in redox state. Results in Figure 3 show that in the presence of non-limiting levels of metabolic substrate, that is at 5 and 20 mM sodium acetate, and with the electrode poised at 0 V, cytochromes are observed mostly in the reduced redox state. This is supported by the position of the redox markers ν_{21}, ν_4, and ν_{20} centered at around 1311 cm^{-1}, 1360 cm^{-1}, and 1392 cm^{-1} (Table S1), which match closely the position of the same marker bands as recorded in the absence of metabolic substrate and with the electrode poised at -0.6 V, conditions at which cytochromes are almost completely reduced (see Table 1). Interestingly, the position of the marker

bands is virtually identical at any distance from the electrode surface, suggesting the absence of a measurable redox gradient across the biofilms, even in proximity to the electrode. Increasing the driving force by poising the electrode potential to 0.2 V did not resulted in appreciable changes in the redox state or in the appearance of a measurable redox gradient (Figure 3b). In fact, on average the bands ν_{21}, ν_4, and ν_{20} were centered at around of 1311, 1359, 1392 cm^{-1} in 5 mM acetate, and 1311, 1360, and 1392 cm^{-1} in 20 mM acetate (Table S1). It was not until we performed measurements in the presence 1 mM of acetate in the bulk liquid that we noticed appreciable shifts in position of the marker bands suggesting significant changes in the redox state of cytochrome (Figure 3). In fact, in this case the relative position of the bands ν_{21}, ν_4, and ν_{20} is consistent with cytochromes in completely oxidized state. Diffusional limitations for substrates within the biofilm were likely irrelevant for acetate levels in the bulk liquid of 5 mM and 20 mM, as it was also suggested previously.[41] It is worth noting that no significant increase of steady-state current followed the increase in the acetate concentration from 5 to 20 mM at both employed potentials (Figure S6), confirming that the whole biofilm performed at the maximal allowed conversion rates and therefore, local variations of the respiration rates due to substrate limitations can be excluded.

Analysis of electron transfer kinetics

The results presented above, specifically, the fact that the oxidation of OMCs lags significantly behind changes in electrode potential, and the absence of a measurable concentration gradient of oxidized (and reduced) cytochromes across the biofilms under turnover conditions, suggests that the limiting step for the electron transfer process in the electroactive microbial community studied here may lay at the biofilm/electrode interface, contrary with what has been observed also using CRRM on *G. sulfurreducens* films grown on gold,[11] and ITO electrodes.[16] In these studies the presence of a measurable redox gradient suggested that the step that limits the overall electron transport is the long-range, homogeneous ET, as opposed to a very fast heterogeneous ET at the biofilm/electrode interface. Currently accepted models for electron transfer across a conductive biofilm matrix describe the catalytic acetate oxidation as

the combination of numerous processes, each accounting for a particular electron transfer step.[18,42] Steps include 1) the mass transport of acetate into the microbial cells, 2) its internal turnover and 3) the reduction of ET mediators (identified here as OMCs) (steps 1 to 3 in Strycharz *et al*.[18]); followed by 4) homogeneous electron transfer through the biofilm matrix via a sequence of ET reactions between fixed mediators (*e.g.,* electron hopping), and 5) the final heterogeneous electron transfer to the electrode by the oxidation of mediators at the biofilm/electrode interface (steps 4 and 5 in Strycharz *et al*.[18]). When used to describe catalytic acetate oxidation of *G. sulfurreducens* biofilms, this model identified non-limiting heterogeneous electron transfer kinetics (step 5 above), while identifying the long-range electron transfer across the biofilm matrix (step 4) and metabolic substrate conversions (steps 1 to 3) as the main rate-limiting steps.[18,42] Conversely, results presented recently by others, suggest that differences might exist between mixed and pure culture electroactive biofilms in the identity of the rate-limiting ET steps. For example, using time-resolved surface-enhanced resonance Raman scattering (SERRS), Ly *et al.*[43] probed selectively the redox states of the OMCs at the biofilm/electrode interface, reporting that the heterogeneous ET was a very slow process (having a k_{ET} = 0.03 s^{-1}) that was coupled with a slightly faster long-range ET (homogeneous) having a predicted rate constant k_{hom} of 1.2 s^{-1}.

To provide a deeper insight into the ET rates of mixed culture biofilms, we applied a combined experimental approach consisting of monitoring the changes of oxidation states of the OMCs in time by means of CRRM during the application of a potential step from an initial (E_i) to a final potential (E_f), the latter process being probed by chronoamperometry (CA). We used the subsequent relaxation of the current profile as indicative of all redox processes occurring in the bulk biofilm and at the biofilm/electrode interface, while we used the relaxation of the intensity of the RR spectra binned at the band ν_{15} at 750 cm^{-1} to monitor long-range electron transfer involving homogeneous transfer between OMCs at a portion of the biofilm at a specific distance from the electrode (fixed at 5 μm from the electrode surface on all measurements). The choice of the marker band ν_{15} at 750 cm^{-1} was dictated

by its relation to the amount of cytochromes in the reduced state. We used a similar approach previously to monitor dynamic variations of heme redox-state during combined voltammetry and RR measurements.[20]

Figure 4 reports typical measurements performed using a potential step with amplitude of 0.7 V from an initial E_i of -0.5 V (which was maintained for 300 s prior to the transition) to a final E_f of +0.2 V (maintained for 240 s after the transition). The E_i was intentionally chosen lower than the average $E_{1/2}$ as determined by non-turnover voltammetry and equal to -0.346 V (*vide supra*), to initiate the transition from a largely reduced redox state of the OMCs. The CA traces of current *vs* time in the absence of acetate after the transition (t > 300 s) display an exponential relaxation phase which levels off towards zero (Figure 4b). Conversely, in the presence of acetate the current traces display a fast discharge process in the instants immediately after the transition (within a few seconds past t = 300 s), which is then superimposed by an electron producing process that levels off towards an average steady-state catalytic current of (41.8±0.1) μA in the later stages of the measurements (Figure 4a). Interestingly, analogous profiles were obtained also during CA tests using a final E_f of 0 V, hence a smaller driving force (Figure S7). Busalmen and coworkers obtained similar profiles of current *vs* time on *G. sulfurreducens* grown on graphite electrodes under turnover conditions, albeit with different time spans.[42,44] The authors described the turnover current as due to the simultaneous contribution of two processes: 1) the reoxidation of the cytochromes reduced in the phases preceding the transition, which is responsible for the initial fast discharge, and 2) the current deriving from the metabolism of acetate, which lags behind the first process, at least for the first instants after the transition, probably due to the requirement for acetate to be transported into the microbial cells before being metabolized. Using a similar conceptual approach, we can consider the turnover current ($i_{turnover}$) as due to the combination of all electron transfer steps (*i.e.*, steps 1 to 5 in Strycharz *et al.*[18]), while the non-turnover current ($i_{non\text{-}turnover}$) as due to the combination of homogeneous and heterogeneous ET alone because of the absence of acetate in the medium (*i.e.,* steps 4 and 5 in Strycharz *et al.*[18]). Therefore, the shape of the difference curve $i_{turnover} - i_{non\text{-}turnover}$ accounts for the contributions

of acetate metabolism alone (Figure 5). The shape of this amperometric trace accounts for steps 1 to 3 in Strycharz *et al*.,[18] that is, acetate uptake into the microbial cells, its metabolic oxidation, and ET to the matrix OMCs. The analysis of this amperometric profile suggests that the discharge current prevails over the metabolic current for a very short time after the transition. At about t = 301 s – thus much earlier than the complete oxidation of the OMCs occurs – the current increases due to the microbial metabolism of acetate. The trace also displays the presence of a local maximum at about 309 s (that is 9 s after the transition). It is possible that this maximum is due to the electrons generated by the oxidation of the acetate that had already entered the microbial cells in the phases prior the transition, when the potential was more negative than that required for the catalytic acetate oxidation. After this internal pool is exhausted (at t > 309 s), however, the production rate of additional electrons will depend on the rate-limiting steps between the transport of new acetate into the cells, its subsequent oxidation, and ET to OMCs. This process is probably regulated by the internal metabolism of the microbes, since changes in gene expression are unlikely within the timeframes observed. Hence, is possible that the presence of the minimum in electric current output at about 319 s is due to the initial need by the organisms to sense the change in potential, and adjust the internal metabolic machinery to the new redox conditions as imposed by the transition to E_f. Recent findings reporting the ability of metal-respiring bacteria to sense the electric field – a property called electrokinesis – forces us to consider that this possibility occurs also in the case of our mixed cultures.[45]

Examination of the CRRM spectra corroborates the interpretation provided above. First of all, analysis of the intensity of the band ν_{15} (Iν_{15}) during the transition experiments (also reported in Figure 4) shows that prior to the potential step (t < 300 s) under both turnover and non-turnover conditions, the redox state of OMCs is mostly reduced. This is inferred by the high intensity of the band ν_{15} (Figure 4a and 4b), as well as by the position of the redox markers ν_{21}, ν_4 and ν_{20} in the RR spectra collected during the 60 seconds prior the application of the transition (spectrum 1 and 3 in Figure 4c and 4d), which proves that the transition starts with OMCs mostly in the reduced state.

This is not surprising since OMCs can store negative charge from the intracellular metabolism under conditions at which the anode cannot act as the electron sink.[42,44,46,47] Our data show that the cell metabolism refills the OMCs before their complete discharge occurs at the electrode. In other words, steps 1-3 are faster than steps 4-5. Our CRRM data confirm this interpretation. In fact, upon the application of the oxidizing potential E_f (+0.2 V), the profile of Iν_{15} *vs* time under non-turnover condition relaxes towards zero very quickly, indicating a shift in the redox state of the cytochromes at 5 μm from the electrode surface to mostly the oxidized state. This is confirmed by the shifts of the bands ν_{21}, ν_4 and ν_{20} to 1314, 1367, 1401 cm^{-1}, respectively, as well as by the presence of the band ν_{10} at 1634 cm^{-1} (Figure 4d). This observation is coherent with the complete discharge of the OMCs in the absence of acetate (*vide supra*). Conversely, under turnover conditions, instead of the exponential decay as displayed in the absence of acetate, the profiles of the Iν_{15} *vs* time show a very sharp initial drop occurring within seconds after the transition (Figure 4a), after which, instead of relaxing to zero as observed in non-turnover, the Iν_{15} rests at an intermediate value ≠ 0 for the remaining of the observations, consistent with an incomplete discharge of the OMCs. Analysis of individual RR spectra collected after the transition, in particular, position and intensity of the bands ν_{21}, ν_4, ν_{20}, and ν_3 (virtually unchanged after the transition), and the absence of the band ν_{10} confirmed the redox state of the OMCs as predominantly reduced, in spite of the partial reduction of intensity of the ν_{15} band (spectra 1 and 2 in Figure 4c). The initial drop observed in the Iν_{15} is likely ascribed to the initial discharge that prevails in the instants right after the transition over the electrons produced by the microbial metabolism, as discussed earlier. However, after this initial phase, electrons from the microbial metabolism will feed to the bulk OMCs, keeping them (mostly) in the reduced redox state. The absence of a transient phase in the Iν_{15} profile similar to that observed for the profile of $i_{turnover}$ (and the $i_{turnover}$ – $i_{non\text{-}turnover}$) before reaching steady-state, suggests that the two processes are not perfectly coupled. Even if the reason for this is unknown, we cannot exclude the contributions of other redox mediators promoting the electron transfer and thus increasing the electrocatalytic current.

Overall, these observations are in line with a scenario whereby in the presence of acetate (and under potentiostatic conditions), electrons are transferred from the microbial central metabolisms to the external OMCs at a rate that is faster than the rate at which electrons travel across the conducting biofilm matrix through hopping between adjacent OMCs (that is, the homogeneous ET as defined above). This scenario requires the rate constant for homogeneous ET k_{hom} to be smaller than the rate constant for the combined metabolic turnover rates k_{mic} (which would be the rate-limiting step between acetate diffusion, acetate oxidation, and electron transfer to the OMCs), that is $k_{mic} > k_{hom}$. In fact, a scenario characterized by sluggish microbial kinetics combined to a fast homogeneous transfer (*i.e.*, $k_{mic} < k_{hom}$) is not consistent to the presence of cytochromes mostly in the reduced redox state as we observed during the transient CA test under turnover conditions ($I\nu_{15}$ trace in Figure 4a). Under these conditions, the rate-limiting process for ET would be either the homogeneous ET or the heterogeneous ET, or the combination of both. Previous analysis by Ly *et at*. suggested that the bulk ET is faster than the interfacial process ($k_{hom} > k_{het}$). This is consistent with our measurements (which cannot exclude, however, $k_{hom} \approx k_{het}$). In fact, a scenario consisting of a sluggish ET in the biofilm and a much faster interfacial electron transfer (*i.e.*, $k_{hom} << k_{het}$) would not have made possible for the bulk OMCs as probed by CRRM to be completely oxidized during the CA test in non-turnover conditions, and it would have resulted in the generation of an appreciable concentration gradient of oxidized OMCs within the biofilms, consistent to CRRM observations on *G. sulfurreducens*.[11,16] Both our measurements at steady-state and during the transient CA experiments do not seem to support such a scenario (*vide supra*). CRRM measurements performed on biofilms comprised of individual cell clusters, which therefore exclude the contribution of multiple cell layers to the redox state of the OMCs in proximity of the interface, are also consistent to the proposed scenario of a sluggish heterogeneous ET (data not shown).

Analysis of the apparent electron transfer rate constant for homogeneous ET

Contrary to the method by Ly *et al*. based on SERRS, our approach based on CRRM does not allow for the direct measurement of the interfacial ET process

due to the physical impossibility to focus the laser beam only on the interfacial OMCs: in fact, being the thickness of the beam typically in the micrometer range, it exceeds by far the thickness of the surface-confined OMCs (< 10 nm). Discerning the contribution of the homogeneous ET from the heterogeneous ET from the current *vs* time trace in non-turnover conditions was also not possible, since the current traces results from the contribution of all ET processes in the whole biofilm.[5] However, we focused here on the examination of the long-range ET process using the analysis of the relaxation profiles of the $I_{\nu 15}$ *vs* time after the transition. In fact, the relaxation constant for the biofilm-embedded OMCs during the transient CA tests described above can be determined by fitting of a single exponential decay function to the profile of the $I_{\nu 15}$ *vs* time. By applying different E_f, it was possible to determine the apparent *k* for homogeneous ET relatively to different driving forces (ΔV). The fitting exercise yielded k_{hom} of (0.038±0.004), (0.043±0.021), and (0.066±0.026) s^{-1} (averages ± standard deviation for triplicate measurements) for the potential steps with E_f of -0.2 V, 0 V, and +0.2 V. Results are presented in Figure 6. Best fitting of the data was achieved with an exponential function (coefficient of determination R^2 = 0.93). The theoretical *k* value determined by imposing the condition of zero overpotential to the fitting curve (that is, for a hypothetical potential step where $E_f = E_{1/2}$ = -0.346 V (see Figure 1)) is, according to the Butler-Volmer formalism, the rate constant at equilibrium, k^0_{hom} (Figure 6). The analysis yielded a k^0_{hom} of 0.028±0.069 s^{-1} (mean ± 95% confidence interval). This is 60 times lower than that predicted by Ly and coworkers under the hypothesis that long-range electron transfer is promoted by only OMCs in the bulk biofilm,[43] and may indicate the contribution of redox mediators other than OMCs to the long-range ET. In our systems, comparison of the measured with the k_{hom} with the hypothetical profile of k^{BV}_{hom} *vs* ΔV as predicted by the Butler-Volmer equation for the same value of k^0_{hom} shows that the observed homogeneous ET is indeed much slower than that predicted by the model (see Figure S8 in the SI). While a weak dependency of ET rates with driving force is characteristic of electron transfer via a hopping mechanism[48] and it was used previously to establish the dominance of inelastic hopping over

tunneling,[43,49,50] our results can be considered consistent to the simultaneous interplay of a fast ET process with a much slower ET mechanism. While the slow ET process could still be ascribed to hopping between adjacent cytochromes, alternative fast ET pathways can perhaps include tunneling between cytochromes with more favorable orientation and/or at closer proximity with each other, or the involvement of alternative ET modes such as bacterial nanowires with metallic-like conducting properties as proposed for networks of *G. sulfurreducens*.[51] It is important to note that the large signal-to-noise ratio that characterizes the real-time CRRM measurements (see for example the $I_{\nu_{15}}$ profiles in Figure 4, 6 and S7) may not permit to discriminate with sufficient accuracy between fast and slow ET processes involving OMCs (*i.e.*, the $I_{\nu_{15}}$ traces account for the macroscopic redox response of the probed sample). On the other hand, the lack of additional information on the biofilm architecture and composition does not permit to be resolute on this aspect at this stage. For example, CRRM is not capable to detect the presence of cellular components such as nanowires or other potentially important redox active molecules in the biofilms examined unless they generate a detectable Raman signal.

Conclusions

By using a specifically designed spectroelectrochemical cell that utilized transparent ITO electrodes, it was possible to assess the redox chemistry of mixed culture electroactive biofilms *in situ* and *in vivo*. Our results show that in the presence of non-limiting levels of metabolic substrate, the oxidation state of OMCs embedded in the biofilm matrix lags significantly behind the electrode potential (contrary to measurements in substrate-depleted medium). Under the same conditions, the redox state of OMCs is mostly reduced at any distance from the electrode surface, even when the electrode is poised at potentials sufficiently high to determine complete oxidation of the OMCs in the absence of substrate. CRRM analysis during potential step transitions under turnover and non-turnover conditions suggested that the respiration rate is a fast process compared to both long-range and interfacial electron transfer processes. Thus, in mixed community biofilms grown on ITO, a fast metabolic

608 acetate respiration feeds electrons to the OMC coupled with much slower or
609 comparable homogeneous ET between OMCs in the conducting biofilm
610 network, and heterogeneous electron transfer at the interface.

611 Acknowledgements

612 This work was performed in part at the Queensland node of the Australian
613 National Fabrication Facility, a company established under the National
614 Collaborative Research Infrastructure Strategy to provide nano- and micro-
615 fabrication facilities for Australia's researchers. BV, BCD, and JOK
616 acknowledge the financial support for CEMES through The University of
617 Queensland. BV acknowledges the support of the UQ Biomedical ECR grant.
618 DM acknowledges the Netherlands Organisation for Scientific Research
619 (NWO) grant 722.011.003.

Figures and Tables

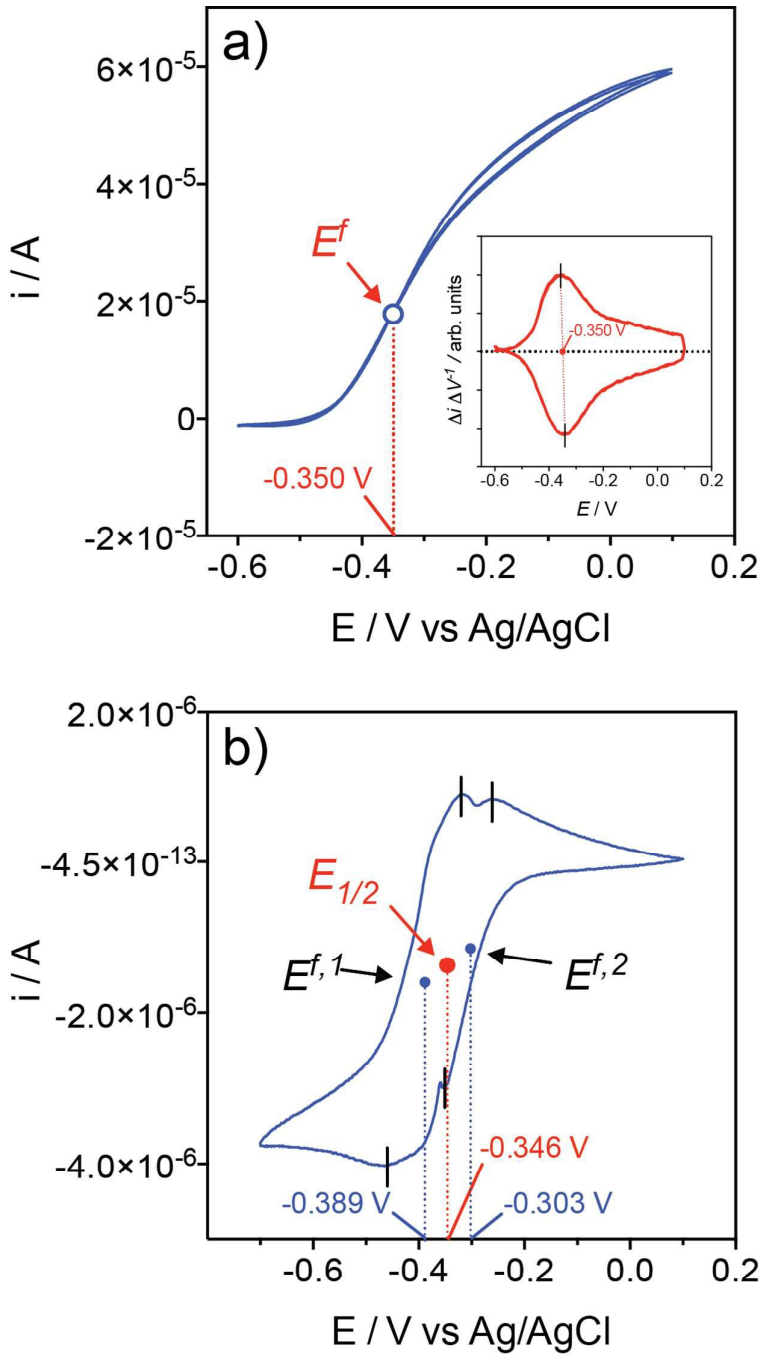

Figure 1. Typical cyclic voltammograms on the electroactive biofilms recorded at the scan rate of 1 mV s^{-1}. a) Turnover CV recorded in the presence of acetate (20 mM), where E^f indicates the putative electron transfer site centered at -0.364 V. Insert indicated the first derivative of the turnover CV. b) Non-turnover CVs in acetate-depleted medium, where $E_{1/2}$ centered at -0.346 V indicates the arithmetic average of two redox couples $E^{f,1}$ and $E^{f,2}$.

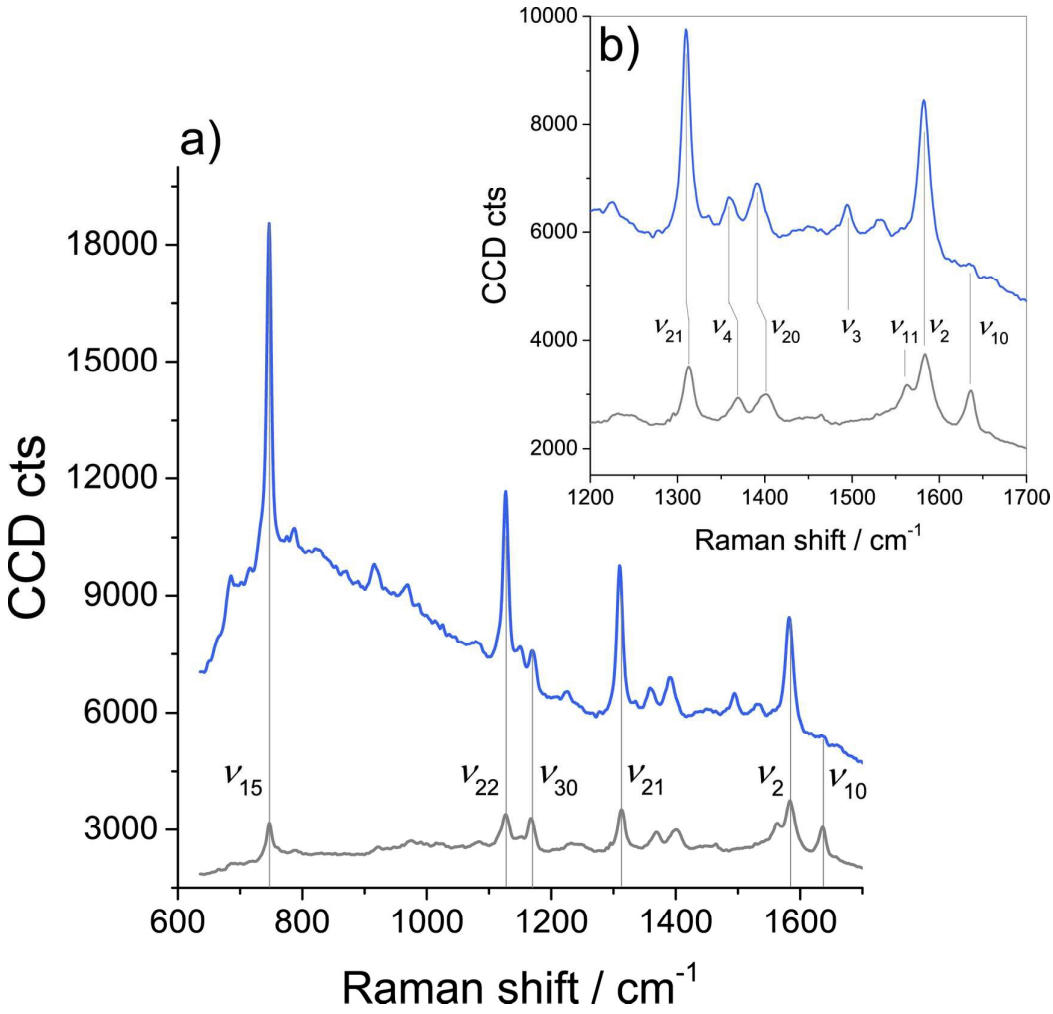

Figure 2. RR spectra of electroactive biofilms in acetate-depleted medium (average of multiple measurements) in a) the spectral region between 600 and 1700 cm^{-1} and b) magnification on the region between 1200 and 1700 cm^{-1}. RR spectra were recorded with the anode potential poised at -0.6 V (blue line) and 0 V (grey line). Relative positions of the marker bands indicated in the figure are reported in Table 1.

635 **Table 1.** Normal mode assignment of the most prominent bands from the averaged Raman
636 spectra obtained with the working electron poised at 0 V and -0.6 V shown in Figure 2.

Band assignment [a]	RR bands at 0V (cm^{-1})	RR bands at -0.6V (cm^{-1})
ν_{15}	747	746
ν_{22}	1127	1127
ν_{30}	1167	1165
ν_{21}	1313	1310
ν_{4}	1369	1360
ν_{20}	1400	1391
ν_{3}	-	1494
ν_{11}	1563 [b]	-
ν_{2}	1583	1582
ν_{10}	1635	1635

[a] assignment accordingly to Hu *et al.*[52]

637 [b] shoulder.

638

639

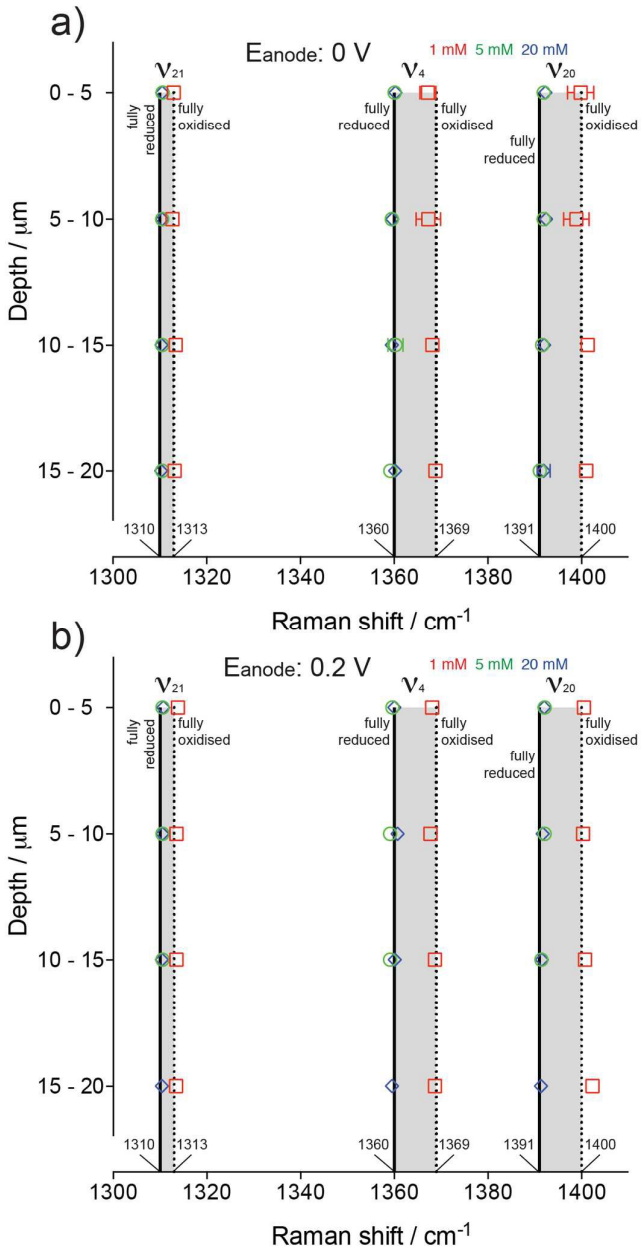

Figure 3. Depth profiling under turnover conditions in media containing acetate: 1 mM (red squares), 5 mM (green circles), and 20 mM (blue diamonds). Measurements performed with the working electrode poised at 0V or +0.2V. The symbols depict the position of the redox markers ν_{21}, ν_4, and ν_{20} as a function of the depth position. RR spectra were collected as 12 single spectrum acquisitions along a 60 μm line in the Z direction with an integration time of 20 s per point. Points were then grouped in discrete intervals of 5 μm and averaged (refer to the SI for details). Note that point Z = 0 μm corresponds to the biofilm/ITO interface, determined as described in the SI. Note that symbols for the data at 5 and 20 mM overlap in some instances. Standard deviations values are in many instances smaller than the symbols, hence, average and standard deviations are also reported in Tables S1 and S2 in the SI.

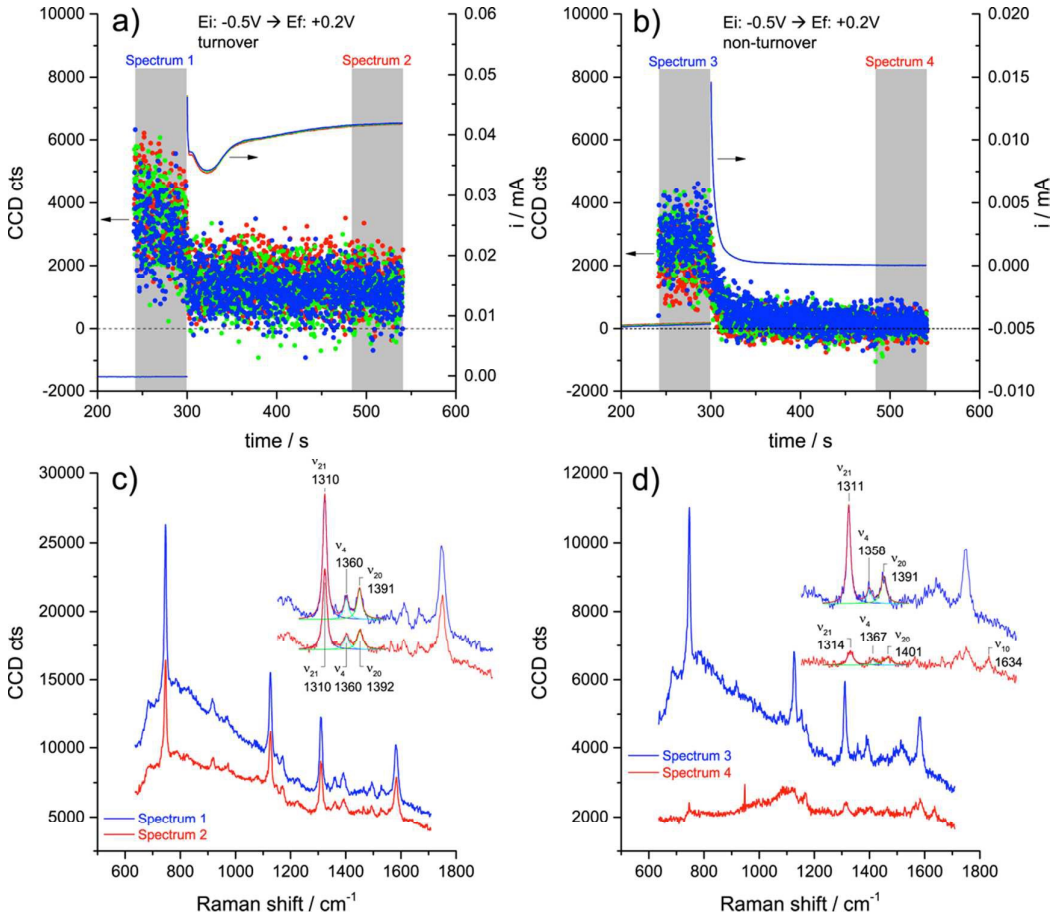

651

652 **Figure 4**. CRRM and Chronoamperometry measurements for potential step with E_i = -0.5 V to
653 E_f = +0.2 V. a) Current *vs* time and intensity of the band ν_{15} *vs* time during the test under
654 turnover and b) non-turnover conditions. c) and d) RR spectra recorded during a 60 s
655 accumulation before the transition (spectra 1 and 3) and 3 minutes after the transition
656 (spectra 2 and 4) during c) turnover and d) non-turnover measurements. Inserts in c) and d)
657 show magnification to the redox markers region and shows relative position of the bands ν_{21},
658 ν_4, ν_{20}, and ν_{10}.

659

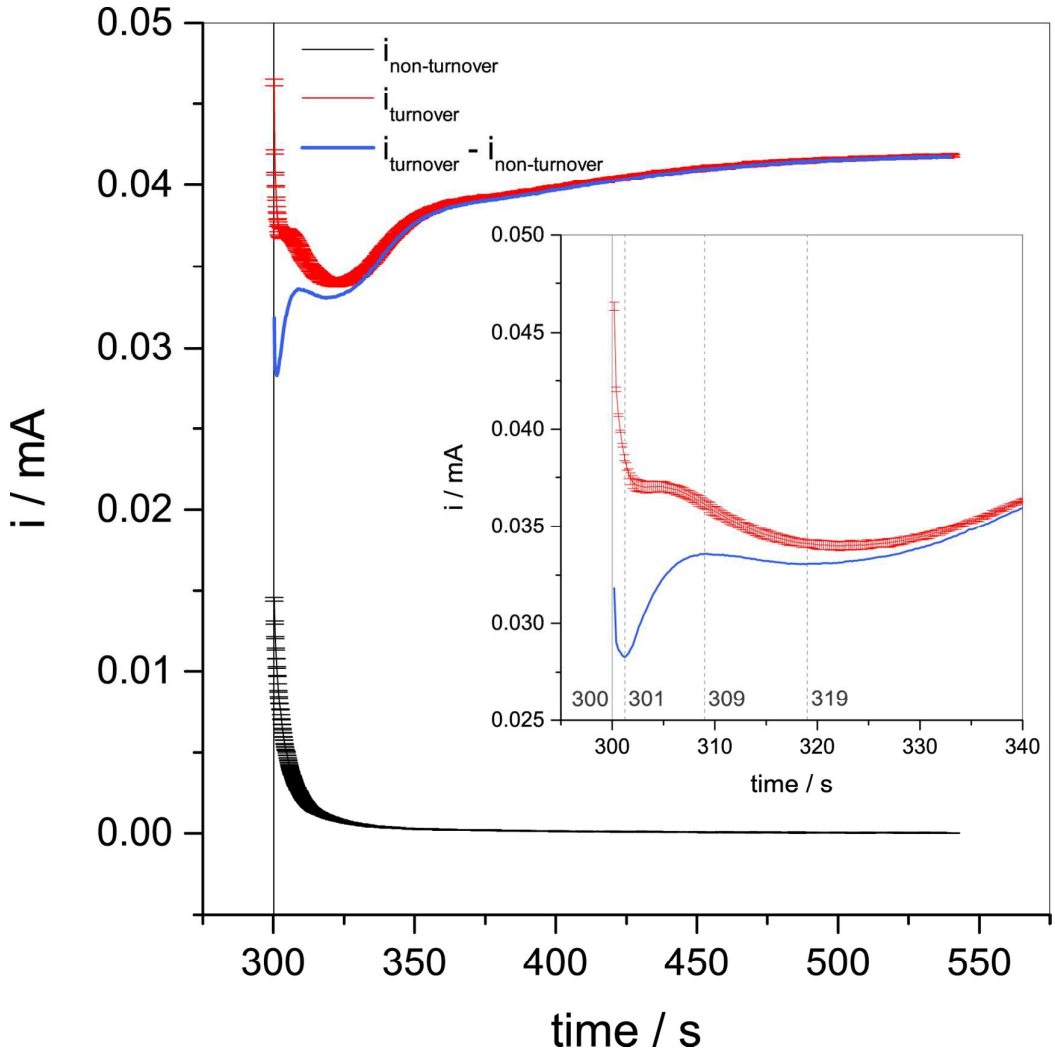

Figure 5. Turnover ($i_{turnover}$) and non-turnover ($i_{non\text{-}turnover}$) current *vs* time traces (averages and standard deviations of the three CA profiles reported in Figure 4) for a potential step with E_i = -0.5 V to E_f = +0.2 V. The calculated trace $i_{turnover} - i_{non\text{-}turnover}$ represents the current due to acetate metabolism alone (see text).

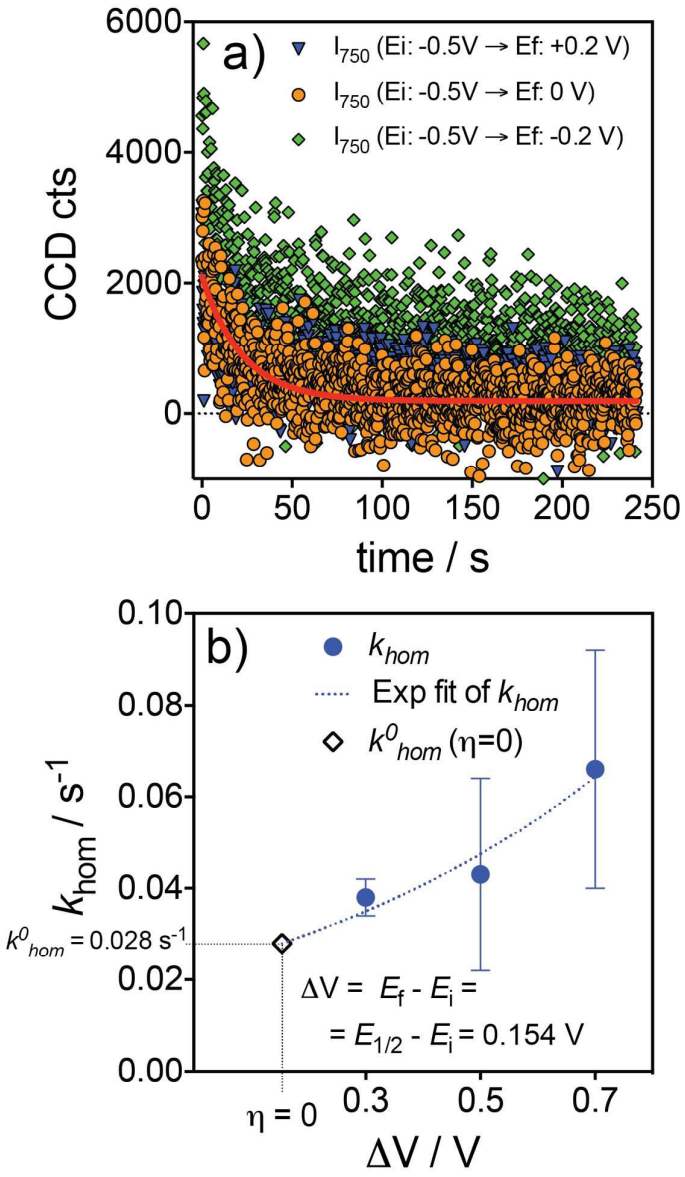

Figure 6. Chronoamperometry performed in non-turnover conditions. a) Relaxation profiles of the intensity of the band ν_{15} *vs* time after the transition from E_i to E_f where E_i = -0.5 V and E_f = -0.2V, 0V, and +0.2V. Values of k_{hom} were evaluated by fitting the relaxation profile of the intensity of the redox marker mode ν_{15} with a monoexponential decay function (an example for E_f = 0 V is indicated in the figure). b) Dependence of the apparent electron-transfer rate constants for homogeneous ET (k_{hom}) on the driving force ($\Delta E = E_f - E_i$). Values are reported as means ± standard deviations for triplicate measurements. The values of k_{hom} as a function of the driving force were fit with an exponential function to determine the k_{hom} at zero overpotential (η=0) - that is, for an hypothetical step where $E_f = E_{1/2}$ = -0.346 V - which corresponds to the rate constant at equilibrium, k^0_{hom}. The fitting yielded k^0_{hom} = (0.028±0.069) s^{-1} (average ± 95% confidence interval).

References

1 S. M. Strycharz, R. M. Snider, A. Guiseppi-Elie and L. M. Tender, *Energ Environ Sci*, 2011, **4**, 4366–4379.

2 N. Malvankar, M. T. Tuominen and D. Lovley, *Energ Environ Sci*, 2012, **5**, 6247–6249.

3 S. M. Strycharz and L. M. Tender, *Energy Environ. Sci.*, 2012, –.

4 S. Pirbadian and M. El-Naggar, *Phys Chem Chem Phys*, 2012, **14**, 13802–13808.

5 N. Malvankar, M. Vargas, K. P. Nevin, A. Franks, C. Leang, B.-C. Kim, K. Inoue, T. Mester, S. F. Covalla, J. P. Johnson, V. M. Rotello, M. T. Tuominen and D. Lovley, *Nature Nanotech*, 2011, **6**, 573–579.

6 D. R. Bond, S. M. Strycharz, L. M. Tender and C. I. Torres, *ChemSusChem*, 2012.

7 N. Malvankar, M. T. Tuominen and D. Lovley, *Energ Environ Sci*, 2012.

8 M. Vargas, N. Malvankar, P.-L. Tremblay, C. Leang, J. A. Smith, P. Patel, O. Synoeyenbos-West, K. P. Nevin and D. Lovley, *mBio*, 2013, **4**.

9 C. Leang, X. Qian, T. Mester and D. Lovley, *Appl Environ Microbiol*, 2010, **76**, 4080–4084.

10 J. P. Busalmen, A. Esteve-Nunez, A. Berna and J. M. Feliu, *Angew. Chem. Int. Ed. Engl.*, 2008, **47**, 4874–4877.

11 N. Lebedev, S. M. Strycharz and L. M. Tender, *Chemphyschem*, 2014.

12 Y. Liu and D. R. Bond, *ChemSusChem*, 2012, **5**, 1047–1053.

13 Y. Liu, H. Kim, R. R. Franklin and D. R. Bond, *Chemphyschem*, 2011, **12**, 2235–2241.

14 D. Millo, F. Harnisch, S. A. Patil, H. K. Ly, U. Schröder and P. Hildebrandt, *Angew. Chem. Int. Ed. Engl.*, 2011, **50**, 2625–2627.

15 H. Richter, K. P. Nevin, H. Jia, D. A. Lowy, D. Lovley and L. M. Tender, *Energ Environ Sci*, 2009, **2**, 506–516.

16 L. Robuschi, J. P. Tomba, G. D. Schrott, P. S. Bonanni, P. M. Desimone and J. P. Busalmen, *Angew. Chem. Int. Ed. Engl.*, 2013, **52**, 925–928.

17 R. M. Snider, S. M. Strycharz, S. D. Tsoi, J. S. Erickson and L. M. Tender, *Proceedings of the National Academy of Sciences*, 2012, **109**, 15467–15472.

18 S. M. Strycharz, A. P. Malanoski, R. M. Snider, H. Yi, D. Lovley and L. M. Tender, *Energ Environ Sci*, 2011, **4**, 896–913.

19 S. M. Strycharz and L. M. Tender, *ChemSusChem*, 2012, **5**, 1106–1118.

20 B. Virdis, D. Millo, B. C. Donose and D. J. Batstone, *PLoS ONE*, 2014, **9**, e89918.

21 M. Estevez Canales, A. Kuzume, Z. Borjas, M. Füeg, D. Lovley, T. Wandlowski and A. Esteve-Nunez, *Env Microbiol Rep*, 2014, **7**, 219–226.

22 S. M. Strycharz, J. Roy, D. Boyd, R. Snider, J. S. Erickson and L. M. Tender, *CHEMELECTROCHEM*, 2014, **1**, 1957–1965.

23 P. S. Bonanni, D. Massazza and J. P. Busalmen, *Phys Chem Chem Phys*, 2013, **15**, 10300–10306.

24 P. Ledezma, P. Kuntke, C. J. N. Buisman, J. Keller and S. Freguia, *Trends Biotechnol*, 2015, **33**, 214–220.

25 B. E. Logan and K. Rabaey, *Science*, 2012, **337**, 686–690.

26 M. T. Agler, B. A. Wrenn, S. H. Zinder and L. T. Angenent, *Trends Biotechnol*, 2011, **29**, 70–78.

27 D. Millo, *Biochem. Soc. Trans.*, 2012, **40**, 1284–1290.

28 B. Virdis, F. Harnisch, D. J. Batstone, K. Rabaey and B. C. Donose, *Energ Environ Sci*, 2012, **5**, 7017–7024.

29 H. Lu, A. Oehmen, B. Virdis, J. Keller and Z. Yuan, *Water Res*, 2006, **40**, 3838–3848.

30 V. Flexer, M. Marque, B. C. Donose, B. Virdis and J. Keller, *Electrochim Acta*, 2013.

31 K. Fricke, F. Harnisch and U. Schröder, *Energ Environ Sci*, 2008, **1**, 144–147.

32 A. Jain, G. Gazzola, A. Panzera, M. Zanoni and E. Marsili, *Electrochim Acta*, 2011, **56**, 10776–10785.

33 A. Okamoto, K. Hashimoto and R. Nakamura, *Bioelectrochemistry*, 2012, **85**, 61–65.

34 B.-S. Yeo, S. Maedler, T. Schmid, W. Zhang and R. Zenobi, *J. Phys. Chem. C*, 2008, **112**, 4867–4873.

35 N. A. Brazhe, M. Treiman, A. R. Brazhe, N. L. Find, G. V. Maksimov and O. V. Sosnovtseva, *PLoS ONE*, 2012, **7**, e41990.

36 F. Adar, *J. Phys. Chem.*, 1978, **82**, 230–234.

37 A. Kuzume, U. Zhumaev, J. Li, Y. Fu, M. Füeg, M. Estévez, Z. Borjas, T. Wandlowski and A. Esteve-Nunez, *Phys Chem Chem Phys*, 2014, **16**, 22229–22236.

38 M. Abe, T. Kitagawa and Y. Kyogoku, *The Journal of Chemical Physics*, 1978, **69**, 4526.

39 S. Oellerich, H. Wackerbarth and P. Hildebrandt, *J Phys Chem B*, 2002, **106**, 6566–6580.

40 K. Artyushkova, J. A. Cornejo, L. K. Ista, S. Babanova, C. Santoro, P. Atanassov and A. J. Schuler, *Biointerphases*, 2015, **10**, 019013.

41 E. Marsili, J. B. Rollefson, D. B. Baron, R. M. Hozalski and D. R. Bond, *Appl Environ Microbiol*, 2008, **74**, 7329–7337.

42 P. S. Bonanni, G. D. Schrott, L. Robuschi and J. P. Busalmen, *Energ Environ Sci*, 2012, **5**, 6188–6195.

43 H. K. Ly, F. Harnisch, S.-F. Hong, U. Schröder, P. Hildebrandt and D. Millo, *ChemSusChem*, 2013, **6**, 487–492.

44 G. D. Schrott, P. S. Bonanni, L. Robuschi, A. Esteve-Nunez and J. P. Busalmen, *Electrochim Acta*, 2011, **56**, 10791–10795.

45 H. W. Harris, M. Y. El-Naggar, O. Bretschger, M. J. Ward, M. F. Romine, A. Y. Obraztsova and K. H. Nealson, *Proceedings of the National Academy of Sciences*, 2010, **107**, 326–331.

46 A. Esteve-Nunez, J. Sosnik, P. Visconti and D. Lovley, *Environ Microbiol*, 2008, **10**, 497–505.

47 N. Malvankar, T. Mester, M. T. Tuominen and D. Lovley, *Chemphyschem*, 2012, **13**, 463–468.

48 L. J. C. Jeuken, A. K. Jones, S. K. Chapman, G. Cecchini and F. A. Armstrong, *J Am Chem Soc*, 2002, **124**, 5702–5713.

49 T. Morita and S. Kimura, *J Am Chem Soc*, 2003, **125**, 8732–8733.

50 J. Hrabakova, K. Ataka, J. Heberle, P. Hildebrandt and D. H. Murgida, *Phys Chem Chem Phys*, 2006, **8**, 759–766.

51 N. Malvankar, S. E. Yalcin, M. T. Tuominen and D. Lovley, *Nature Nanotech*, 2014.

52 S. Hu, I. K. Morris, J. P. Singh, K. M. Smith and T. G. Spiro, *J Am Chem Soc*, 1993, **115**, 12446–12458.